IEEE Access
Multidisciplinary | Rapid Review | Open Access Journal

Received February 3, 2022, accepted February 13, 2022, date of publication February 15, 2022, date of current version February 22, 2022.

Digital Object Identifier 10.1109/ACCESS.2022.3151858

An Adaptive Handover Scheme for Hybrid LiFi and WiFi Networks

GUANGHUI MA[1], (Graduate Student Member, IEEE), RAJENDRAN PARTHIBAN[2], (Senior Member, IEEE), AND NEMAI KARMAKAR[1], (Senior Member, IEEE)

[1]Department of Electrical and Computer Systems Engineering, Monash University, Melbourne, VIC 3800, Australia
[2]School of Engineering, Monash University Malaysia, Subang Jaya 47500, Malaysia

Corresponding author: Guanghui Ma (guanghui.ma@monash.edu)

ABSTRACT The hybrid light fidelity (LiFi) and wireless fidelity (WiFi) network (HLWNet) is considered to be a potential component of the next generation indoor wireless networks. However, due to the susceptible line-of-sight propagation of optical signal and the ultra-dense deployment of LiFi access points, the handover problem in the HLWNet becomes challenging and it is hard to design a handover scheme that adapts to complex indoor working scenarios. In this paper, we propose a novel handover scheme, in which the handover events in HLWNet are classified into three categories and a particular strategy for each category is applied to calculate the optimal dwell time in the handover procedure. The proposed handover scheme is adaptive to different working situations, since the information about multiple attributes, such as channel quality, user velocity, and arrivals data rate, is gathered to make the handover decision and to calculate the dwell value. The simulation results show that, compared to the benchmarks, the proposed method is able to increase the user throughput by around 65%, decrease the handover rate by up to 80%, and reduce the packet delay by up to 57%. In addition, the proposed method significantly improves the robustness performance of user throughput and handover rate under different scenarios.

INDEX TERMS Handover, heterogeneous network (HetNet), light fidelity (LiFi), wireless fidelity (WiFi), visible light communication (VLC).

I. INTRODUCTION

Mobile data traffic is expected to reach 77 exabytes per month in 2022, when it is predicted that 90% of the global mobile data will be consumed by smart devices and 80% of the data activity will occur indoor [1]. To enable this amount of traffic to be carried, there is an urgent need for an advanced indoor wireless network with faster connections and greater capacity. Visible light communication (VLC) technology and its network variant, light fidelity (LiFi), which use 300THz licence-free and unused spectrum for wireless communication are regarded as promising components of the next generation indoor wireless networks [2].

LiFi has a number of advantages over radio frequency (RF) networks. Firstly, LiFi is more power-efficient and less expensive than indoor RF wireless networks, e.g. wireless fidelity (WiFi), since it uses inexpensive light emitting diodes (LEDs) as access points (APs) which provide illumination and data transmission at the same time. In addition, LiFi has a higher data rate than WiFi does due to its broader optical bandwidth and denser deployment of LEDs [3]. Furthermore, the security of the physical layer can be enhanced as the optical light cannot penetrate through walls and opaque objects. However, LiFi also has a number of limitations. A solo LiFi network has a small coverage area in which user mobility cannot be guaranteed [4]. In addition, the susceptible line-of-sight (LoS) links between LiFi APs and users can be easily disrupted by occasional shadowing and angular misalignments [5]. To enhance user mobility and signal continuity, the concept of the hybrid LiFi and WiFi network (HLWNet) has been introduced [6]. This hybrid network, combining the high-speed data transmission of LiFi and the ubiquitous coverage of WiFi, has been proven to achieve greater throughput and better quality of service (QoS) than a stand-alone LiFi or WiFi network [7]. Despite the

The associate editor coordinating the review of this manuscript and approving it for publication was Li Zhang.

clear advantages of an HLWNet, the handover issue in it becomes more challenging due to the LoS optical signal and ultra-dense deployment of LiFi APs.

Handover is the transfer mechanism between wireless cells that occurs in a device within a call service [8], [9]. Depending on which network the target base station (BS) or AP belongs to, the handover is classified as either horizontal handover (HHO) or vertical handover (VHO). HHO is the handover between the same kind of access networks, whereas VHO is between different types [10]. Since the HLWNet is assumed to be implemented in a medium sized office or classroom, where WiFi can cover the whole area, VHO alone is sufficient for a complete handover scheme in HLWNets [11]. The term handover in this article refers to VHO unless otherwise stated.

The rules of the handover procedure are given by a handover algorithm that plays the most important role in a handover scheme design. There are two basic VHO algorithms, immediate VHO (IVHO) and dwell VHO (DVHO) in heterogeneous VLC and RF networks [12]. As the name suggests, the user equipment (UE) implemented with IVHO will transfer to the RF network immediately once the optical channel is unavailable. Theoretically, IVHO provides the highest user throughput because it is always connected to the AP with the best service. However, this approach causes ping-pong effects and deteriorates the QoS of users. To avoid frequent switching between VLC and RF networks, UEs are designed to wait for a dwell time, during which the handover process will be terminated if the optical channel resumes. The length of dwell time, however, should be set properly. On the one hand, the ping-pong effect cannot be completely solved if the dwell time is too short. On the other hand, a dwell time that is too long will accumulate delay, resulting in the reduction of average throughput. One possible solution is to design a handover algorithm with dynamic dwell which can get updated automatically based on different working scenarios [13].

There has been considerable research investigating the VHO mechanisms in heterogeneous RF and VLC networks. Reference [14] presents a handover scheme that calculates the dynamic dwell time by using the measured information about channel quality and user movement. However, it only considers the signal interruptions caused by user movement; interruptions caused by light-path blockages and device orientation are not taken into account. Reference [15] reports a Q-learning based handover scheme to maximize the average throughput in an office building. In this scheme, an optimized time-to-trigger (TTT) value table is obtained by pre-training and the most appropriate TTT is then distributed to each UE in different time slots. The TTT, which can be regarded as the dwell time, is fixed in a certain time slot in this scheme and is not adaptive to different working environments. To improve the dynamic performance of HLWNets, especially to reduce the handover rate for mobile users, a handover skipping technology using reference signal received power (RSRP) is introduced in [16]. Using this skipping technology, reference [17] proposes a handover method that can reduce the handover rate and also increase the throughput for roaming users with different velocities. However, this method does not taken into account the interruptions caused by light-path blockages and device orientation. To handle the interruptions caused by both UE mobility and optical channel blockages, reference [18] presents a fuzzy logic (FL) based VHO scheme, which uses the instantaneous/average signal-to-interference-plus-noise ratio (SINR), user velocity, and the information about required data rates to make a handover decision. It shows that the UEs implemented with the FL based handover scheme are able to achieve higher user throughput than those with traditional methods do.

From the previous studies, there appear to be at least three categories of VHO events from LiFi to WiFi in HLWNets: *Type I*, VHOs caused by the optical signal instability due to the user's movement; *Type II*, VHOs caused by sudden signal termination due to random shadowing or UE orientation; *Type III*, active handovers that occur when both WiFi and LiFi signals exist but the WiFi is found to offer better QoS. Among these three types of VHOs, *Type I* and *Type II* do not exist in conventional heterogeneous RF networks. Most previous studies such as [14], [15], and [17] can only handle one or two types of VHOs. Reference [18], on the other hand, attempts to handle all types of VHOs holistically; however, it takes long processing time, since its handover process, which contains fuzzification and defuzzification etc., is very complex. In addition, the single FL based handover strategy cannot achieve global optimization as different categories of VHOs have different characteristics.

To obtain optimal overall performance with low complexity, we divide the handover problem in the HLWNet into three subproblems by different categories of VHOs and design a particular handover strategy for each type of VHO event.

In this study, we propose a novel handover scheme that firstly determines the type of the VHO event by the gathered information about channel qualities, user movement, and the arrival data rate. It then calculates the optimal dwell time with a specific strategy for this type of VHOs. The simulation results show that, compared with conventional handover methods and the FL based handover scheme from [18], the proposed scheme is able to increase the transmission rate by around 65%, decrease the handover rate by up to 80%, and reduce the packet delay by up to 57%. In addition, the proposed method is adaptive to different scenarios and shows great robustness performance.

The rest of the paper is organised as follows. Section II introduces the channel model of HLWNets. Section III presents the proposed handover scheme, in which VHOs are divided into three categories, and specific strategies are designed for each category to calculate adaptive dwell time. The simulation results are presented and discussed in Section IV and conclusions are drawn in Section V.

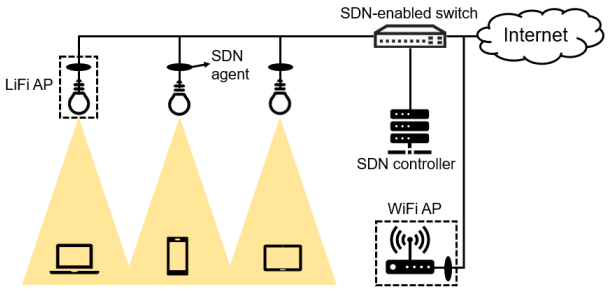

FIGURE 1. A SDN-enabled HLWNet architecture.

II. CHANNEL MODEL

To achieve a flexible access selection and handover process, a software-defined networking (SDN) based network architecture is adopted in our study, as illustrated in Fig. 1 [19], [20] [21]. In this architecture, LiFi and WiFi APs are connected to an SDN-enabled switch via SDN agents and the data packet flow is controlled by the SDN controller. The SDN controller, an application in the SDN architecture, uses protocols to direct switches to send packets. Due to numerous challenges to build an optical uplink, an asymmetrical scheme using both LiFi and WiFi as downlinks and only WiFi as the uplink is applied. Additionally, the two-dimensional (2D) lattice deployment is used. As depicted in Fig. 2, N_A LiFi APs are deployed on the office ceiling in a lattice topology. Meanwhile, a single WiFi AP, which is assumed to cover the whole room, is fixed in the centre among LiFi APs. The sets of UEs (including stationary and roaming ones) and APs are denoted by $\{u \mid u \in [1, N_U]\}$ and $\{a \mid a \in [0, N_A]\}$ respectively, where N_U is the number of UEs being served and $a = 0$ means WiFi AP is being connected. In addition, carrier-sense multiple access with collision avoidance (CSMA/CA) and time division multiple access (TDMA) are respectively implemented in WiFi and LiFi systems for multiple access [22].

A. LiFi CHANNEL MODEL

If the transmitted power from LED a ($a \neq 0$) is $P_{t,a}$, the received power $P_{r,u}$ at UE u can be expressed as,

$$P_{r,u} = H_{u,a} \times P_{t,a}, \tag{1}$$

where $H_{u,a}$ is the channel gain between LiFi AP a and UE u. In the intensity modulation direct detection (IM/DD) method, photons gathered from photodetectors (PDs) will be converted to electric current, expressed as:

$$I_{u,a} = R_{pd} H_{u,a} P_{t,a}, \tag{2}$$

where R_{pd} is the detector responsivity of the receiver. Since light path propagation delay is negligible in indoor scenarios, the optical channel gain $H_{u,a}$ can be defined as,

$$H_{u,a} = H_{u,a}^{LoS} + H_{u,a}^{NLoS} + H_n, \tag{3}$$

where $H_{u,a}^{LoS}$ and $H_{u,a}^{NLoS}$ represent the LoS and non LoS (NLoS) channel gain between u and a respectively; H_n is the addictive white Gaussian noise (AWGN).

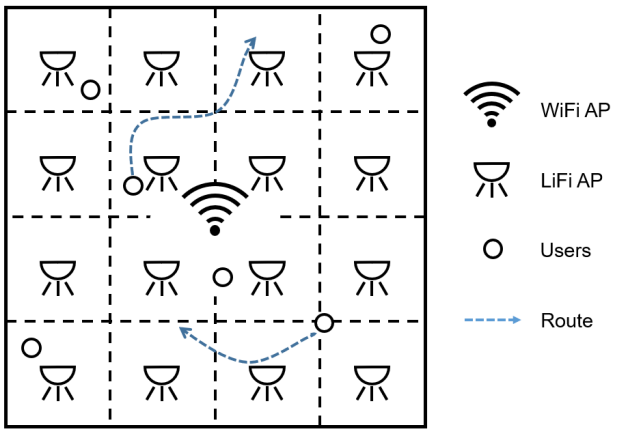

FIGURE 2. Sample AP deployment with 16 LiFi APs, 1 WiFi AP and 6 users.

The LoS channel gain is formulated as [23]:

$$H_{u,a}^{LoS} = \frac{A_{pd} cos(\psi_{u,a})(m+1)}{2\pi d_{u,a}^2} cos^m(\phi_{u,a}) g_f g_c(\psi_{u,a}) \tag{4}$$

where $\phi_{u,a}$ is the irradiance angle and $\psi_{u,a}$ is the incidence angle which is the angle between the incident light and the normal vector n_{pd}, as shown in Fig. 3. The direction of n_{pd} can be described by the polar angle θ and the azimuth angle ω as [22], [24]:

$$n_{pd} = [sin(\theta)cos(\omega), sin(\theta)sin(\omega), cos(\theta)]^T. \tag{5}$$

A_{pd} is the detector area of the receiver and $A_{pd} cos(\psi_{u,a})$ is the effective collection area of the receiver; $d_{u,a}$ is the distance between the LED and the PD; m is the Lambertian emission order, which can be expressed as a function of semi angle of half power $\phi_{1/2}$, $m = -ln2/ln(cos\phi_{1/2})$; g_f is the gain of the optical filter; $g_c(\psi_{u,a})$ is the optical gain of a non-imaging concentrator, expressed as $g(\psi) = n_i^2/sin^2\Psi_{max}$, where n_i is the refractive index, and Ψ_{max} is the field of view of the PD. In [25], the authors show that the high-order NLoS channel gain is negligible to the downlink performance of VLC, so only the first order reflections are considered in this study. The first-order NLoS channel gain is given by Eq. 6, where ρ_w is the reflectivity ratio of the reflection surfaces; A_w is the total reflection area; $\psi_{w,a}$ and $\psi_{u,w}$ are the incidence angles at the point w and UE u respectively [26].

Thus, the SINR for user u and LiFi AP a can be expressed as,

$$\gamma_{u,a} = \frac{(R_{pd} H_{u,a} P_{t,a})^2}{\iota^2 N_{LiFi} B_{LiFi} + \sum_{i \neq a, i>0}^{N_A} (R_{pd} H_{u,i} P_{t,i})^2}, \tag{7}$$

where B_{LiFi} is the bandwidth for each LiFi AP; N_{LiFi} is the power spectral density (PSD) of noise, which is dominated by shot noise [27]. ι is the optical to electric power conversion coefficient.

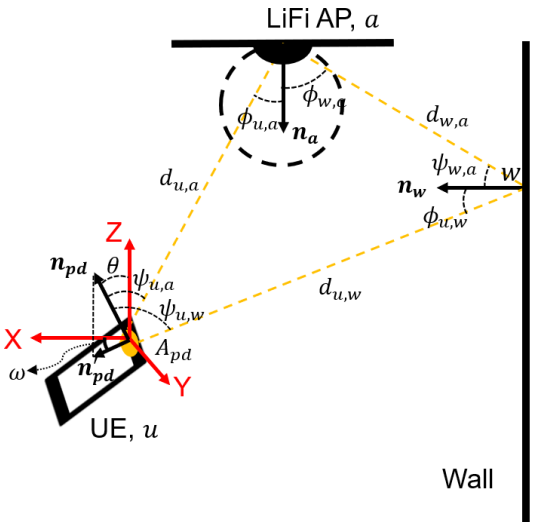

FIGURE 3. The LoS and the first-order reflection NLoS propagation.

B. WiFi CHANNEL MODEL

A 2.4GHz WiFi AP is adopted in our study. The channel gain between the antenna to user u is modelled as:

$$H_{u,0} = L_{WiFi} \times h_{WiFi}, \tag{8}$$

where L_{WiFi} is the path loss caused by large scale obstructions, which is formulated as [28]:

$$L_{dB}(d) = \begin{cases} L_{FS}(d_{u,0}) + SF, & d_u \le d_{BP} \\ L_{FS}(d_{BP}) + 25log_{10}(\frac{d_{u,0}}{d_{BP}}) + SF, & d_u > d_{BP}. \end{cases} \tag{9}$$

It should be noted that the above equations are written in decibels (dB), which means that $L_{dB} = 10log_{10}(L_{WiFi})$; L_{FS} is the free space path loss in dB, expressed as $L_{FS} = 20log_{10}(d_{u,0}) + 20log_{10}(f) - 147.5$, where f equals to 2.4GHz; $d_{u,0}$ is the distance from WiFi antenna to UE u; and the shadow fading, SF, follows a log-normal distribution with zero mean and standard deviation, σ_{SF}. Because an office with the size $(18 \times 18)\text{m}^2$ is chosen as the simulation scenario, the maximum distance from the antenna to the UE is longer than 10m. Thus, the path loss model D in [28] is chosen for the simulation, where breakpoint d_{BP} is equivalent to 10m, and σ_{SF} equals to 3dB and 5dB before and after d_{BP}, respectively.

h_{WiFi} is the channel gain from NLoS components, which is formulated as:

$$h_{WiFi} = (\sqrt{\frac{K}{K+1}} e^{j\phi_0} + \sqrt{\frac{1}{K+1}} X), \tag{10}$$

where the random variable X follows complex Gaussian distribution with zero mean and unit variance; ϕ_0 is the arrival/departure angle of the LoS component; and K is the Ricean K-factor, which equals to 2 when $d_{u,0} < d_{BP}$ and 0 otherwise.

If the transmitted power from WiFi is $P_{t,0}$, the received signal power at u is:

$$P_{r,u} = |H_{u,0}|^2 P_{t,0}. \tag{11}$$

Since interference does not exist in WiFi channel, its SINR, equivalent to signal-to-noise ratio (SNR), is given as:

$$\gamma_{u,0} = \frac{|H_{u,0}|^2 P_{t,0}}{N_{WiFi} B_{WiFi}}, \tag{12}$$

where N_{WiFi} and B_{WiFi} are the noise PSD and bandwidth of the WiFi channel.

C. ACHIEVABLE DATA RATE

Shannon capacity is employed to estimate the data rate provided by the WiFi AP; whilst the lower bound capacity of LiFi channel, derived in [29], is applied to estimate the data rate served by a LiFi AP. Therefore, the the achievable data rate provided by AP a to user u can be expressed as follows:

$$r_{u,a} = \begin{cases} \rho_{u,a} \frac{B_a}{2} log_2(1 + \frac{e}{2\pi} \gamma_{u,a}), & a \neq 0, \text{LiFi} \\ \rho_{u,a} \frac{B_a}{2} log_2(1 + \gamma_{u,a}), & a = 0, \text{WiFi}, \end{cases} \tag{13}$$

where $\rho_{u,a}$ is the proportion of frequency/time resource of AP a used by user u; e is Euler's number. For simplicity, the resource is assumed to be equally shared by all users in AP a [Eq. 10, [30]]. The bandwidth provided by AP a is denoted by B_a.

D. USER BEHAVIOUR MODELING

The most advanced orientation random waypoint (ORWP) is applied to model indoor user behaviours in this study [24], [31]. In this model, the user's dynamic information at any time point n can be denoted as a tuple, $(P_n, v_n, \theta_n), n \in \mathbb{N}$, where $P_n = (x_n, y_n)$ is user's position; v_n and θ_n are the velocity and the polar angle of the mobile device respectively. The time period between two samples, T_s, is not longer than the quasi-static period, during which the channel state information (CSI) of LiFi and WiFi channels is assumed to be constant [32]. To simulate the varying speed behavior of indoor users, the velocity direction, $\frac{v_n}{\|v_n\|}$, and magnitude, $\|v_n\|$, are periodically updated based on certain distributions. As for θ, an experimental measurement based model for device orientation shows that the probability density function (PDF) of the polar angle of a moving user follows a Gaussian distribution with the mean of $\mathbb{E}[\theta] = 29.67°$ and standard deviation of $\sigma_\theta = 7.78°$ [24]. The random process θ_n can be generated by a first order autoregressive model:

$$\theta_n = c_0 + c_1 \theta_{n-1} + w_n, \tag{14}$$

where, w_n is a white noise process with the variance σ_w^2. The factors c_0, c_1, and σ_w^2 can be calculated as follows:

$$c_0 = (1 - c_1)\mathbb{E}[\theta], \quad c_1 = 0.05^{\frac{T_s}{T_c}}, \quad \sigma_w^2 = (1 - c_1^2)\sigma_\theta^2, \tag{15}$$

where T_c set as 130ms, is the coherence time of the random process θ [31]; T_s is the sampling time, which is chosen to be equal to T_c in this paper.

E. LIGHT-PATH BLOCKAGE

Due to the directional propagation of visible light, optical shadowing is another unique phenomenon in LiFi networks. ON-OFF model is used to simulate the light-path blockage in this paper [11], [12] [13]. Assuming that the blockage of the light-path is totally random and that there is no relation between two different blockages, the occurrences of the optical interruptions and resumptions can be described as a Poisson process. In other words, the interruption/resumption occurrences obey a Poisson distribution and its duration is exponentially distributed [33]. If the interruption and recovery rates of the LoS link are ξ_1 and ξ_2, the duration of the VLC availability and unavailability will be exponentially distributed with mean values equal to $\frac{1}{\xi_1}$ and $\frac{1}{\xi_2}$, respectively [13]. For simplicity, the optical received signal strength of the UE is equal to 0 during the blockage and resumes immediately once the optical channel recovers.

III. METHODOLOGY

As mentioned in Section I, since VHOs may be triggered by different events and different types of VHOs have distinguishing characteristics, the authors propose a novel handover scheme, which calculate the optimal dwell time for different categories of VHOs with different strategies. After the review of previous works, we conclude that there exist at least three categories of VHOs from LiFi to WiFi in HLWNets: *Type I*, the VHOs triggered by high velocity; *Type II*, the VHOs caused by unpredictable shadowing or device orientation; and *Type III*, WiFi found to provide better service. *Type III* VHOs are probably triggered by user movement, the fluctuation of arrival data rate, or arrival/departure of new users in LiFi/WiFi APs. To avoid conflicts when two types of VHOs are triggered simultaneously, the priority of different VHO categories from high to low is set as: *Type I* > *Type II* > *Type III*. The dynamic dwell calculation for each type of VHOs will be introduced in the following subsections.

A. TYPE I

This type of VHOs are the most understandable ones. Once user velocity is reported exceeding a certain threshold τ, the LiFi network is no longer preferable since the fast movement leads to optical signal instability and frequent VHOs. At this moment, the *Type I* VHO will be activated and the dwell value will be set as 0, which means to execute the handover to WiFi immediately. Therefore, our first task is to find the the threshold τ that achieves the optimal overall performance for *Type I* handovers. When the light-path and device orientation are not involved, we run the simulation with the same parameters as in Section IV. The plot of average achievable throughput and average handover rate against different choices of τ is shown in Fig. 4. We can find that under our simulation scenario, the optimal velocity threshold for *Type I* handovers are around $1.0-1.4$m/s, where the average user throughput remains high and the handover rate maintains at a low level. In the following sections, we choose $\tau = 1.1$m/s as the optimal threshold for *Type I* handovers. It should be noted that the choice of the optimal threshold depends on the room size, the deployment of the LiFi APs, and the other parameters. Therefore, preliminary experiments are needed to check the τ value in real life.

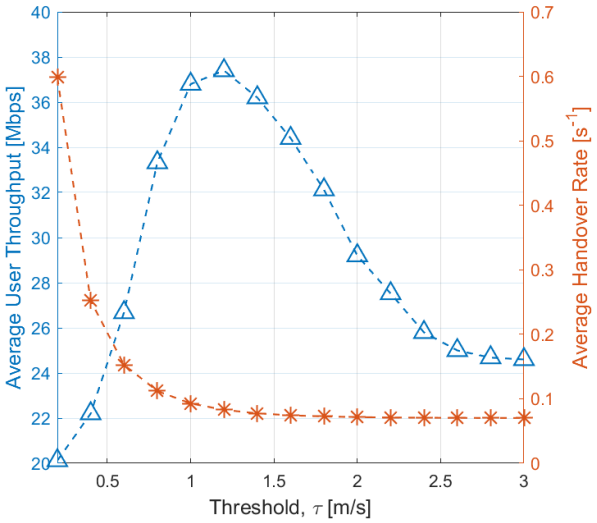

FIGURE 4. Average throughput and handover rate versus τ.

B. TYPE II

If the average SINR for the past M samples of the UE is stable but the instantaneous SINR suddenly drops to a very low value, the optical channel can be assumed to be blocked and a similar SINR value is expected to be obtained after the LiFi channel resumes. Since the optical channel is unavailable in this situation, the goal of the *Type II* strategy is to calculate the optimal dwell time to minimize the delay caused by the interruption, which then will increase the overall throughput.

When the optical channel is disrupted, if IVHO is performed, the delay of UE u will be,

$$\delta_{u,IVHO} = T_{exe} + \frac{\Pi}{r_{u,0}(\overline{\gamma_{u,0}})}, \tag{16}$$

where T_{exe} is the execution time of a handover process; $r_{u,0}$ is the data rate provided by WiFi, which is a function of the SINR of WiFi channel. $\overline{\gamma}$ is the average SINR of past M samples; Π represents the size of delayed packets in buffer during the interruption. Assuming that the buffer queue is long enough, Π has the same magnitude as the arrival data rate [12], [34]. On the other hand, if DVHO is performed, the

$$H_{u,a}^{NLoS} = \int_{A_w} \frac{A_{pd}(m+1)\rho_w}{2\pi d_{w,a}^2 d_{u,w}^2} cos^m(\phi_{w,a}) g_f g_c(\psi_{u,w}) cos(\psi_{w,a}) cos(\psi_{u,w})\, dA_w \tag{6}$$

delay will be,

$$\delta_{u,DVHO} = \begin{cases} T_{exe} + T_{dw} + \frac{\Pi}{r_{u,0}(\overline{\gamma_{u,0}})}, & T_{dw} \leq T_{int} \\ T_{int} + \frac{\Pi}{r_{u,a}(\overline{\gamma_{u,a}})}, & T_{dw} > T_{int}, \end{cases} \quad (17)$$

where T_{dw} is the length of dwell time; T_{int} is the interruption duration; $r_{u,a}$ is the data rate provided by LiFi AP a, which is a function of $\overline{\gamma_{u,a}}$. Comparing Eq. 16 and 17, DVHO is meaningful only if

$$T_{int} + \frac{\Pi}{r_{u,a}(\overline{\gamma_{u,a}})} < T_{exe} + \frac{\Pi}{r_{u,0}(\overline{\gamma_{u,0}})}, \quad (18)$$

i.e. $T_{int} < T_{exe} + \frac{\Pi}{r_{u,0}(\overline{\gamma_{u,0}})} - \frac{\Pi}{r_{u,a}(\overline{\gamma_{u,a}})}$. Furthermore, to avoid ping-pong effects in this scenario, $T_{dw} > T_{int}$ should be satisfied. Thus the optimal dwell time for *Type II* handovers can be set as,

$$T_{dw} = max\{T_{exe} + \frac{\Pi}{r_{u,0}(\overline{\gamma_{u,0}})} - \frac{\Pi}{r_{u,a}(\overline{\gamma_{u,a}})},\ 0\}, \quad (19)$$

which can reduce latency as well as avoid unnecessary handovers. Average SINR of both LiFi and WiFi networks and the delayed packets in the buffer are utilised to estimate the optimal dwell time when the optical channel is blocked, so this dwell time is adaptive to different working situations. In addition, the statistical information of past interruptions is not used, due to the unpredictability of optical channel shadowing.

C. TYPE III

When both LiFi and WiFi are available and user velocity is below the threshold, UEs are preferred to access the AP that can provide the highest average data rate. Different from pure RF networks, where data rates provided by different APs can be compared directly, it is not obvious which AP is the "better" choice in HLWNets. Therefore, we introduce a satisfaction index, $\zeta_{u,a} (\in [0, 1])$, to quantitatively evaluate the QoS of LiFi and WiFi networks. To reduce the algorithm complexity, the set of reachable APs only contains two elements, the LiFi AP with the highest SINR and the WiFi AP, i.e. $a \in \{0, \alpha\}$, where $a = 0$ still represents the WiFi AP; and $\alpha = \arg\max_{a \in [1, N_A] \cap \mathbb{N}} \gamma_{u,a}$. Since user velocity and data rate are two parallel conditions to trigger the handover process, which means either of them can trigger the VHO process, the index $\zeta_{u,a}$ is defined as the product of the normalization of these two metrics, i.e.

$$\zeta_{u,a} = \mathcal{N}_{a,v}(v_u) \times \mathcal{N}_r(r_{u,a}). \quad (20)$$

As we have explained, the LiFi network access is sensitive to user velocity; therefore, the normalization function $\mathcal{N}_{a,v}(\cdot)$ can be chosen as:

$$\mathcal{N}_{a,v}(v) = \begin{cases} \frac{1}{UB_{a,v}}(UB_{a,v} - v) & v \leq UB_{a,v} \\ 0 & v > UB_{a,v}, \end{cases} \quad (21)$$

where the upper bound, $UB_{a,v}$, equals to the optimal threshold τ from Section III-A. Since WiFi has much higher tolerance to human velocity, its normalization value is always equivalent to 1 for indoor users. $\mathcal{N}_r(\cdot)$ is the data rate normalization function, expressed as,

$$\mathcal{N}_r(r_{u,a}) = \begin{cases} \frac{1}{UB_r} r_{u,a} & r_{u,a} \leq UB_r \\ 1 & r_{u,a} > UB_r, \end{cases} \quad (22)$$

where UB_r equals to the arrival data rate, which is a dynamic parameter.

Therefore, $\zeta_{u,a}$ ranges from 0 to 1, and the greater it is, the better the network quality is. The *Type III* handover process will be triggered if the satisfaction index of the target AP is greater than the current one. To avoid the ping-pong effect, we extend the concept of "stability period" from [35] and rewrite [Eq. 3, [35]] as follows.

$$T_{dw} = T_{exe} + \frac{T_{exe}}{Z - 1} \quad (23)$$

This is the dynamic dwell time defined for *Type III* VHOs, where $Z = \frac{\zeta_{u,tgt}}{\zeta_{u,crt}}$ is the ratio of the satisfaction indices of target and current APs. The handover process will be immediately terminated once $Z \leq 1$.

D. SUMMARY

A complete handover scheme contains three modules, as shown in Fig. 5, including information gathering, decision making, and handover execution modules. The information gathering module (IGM), also known as handover initiation or system discovery module, is used to collect all the information required for the handover decision [36]. In our proposed scheme, this module is implemented in the mobile node to monitor SINR values of LiFi/WiFi channel, user velocity, and arrival data rate [15], [21]. Once the handover trigger conditions have been fulfilled, the IGM passes the type of the handover event and the related information to the decision making module (DMM). The DMM firstly calculates the optimal dwell time with the algorithm described in Section III-A,B, and C, and then passes the dwell time to its dwell timer. During the dwell time period, the IGM keeps monitoring the conditions of the UE, and reports the new event to the DMM if a higher-order VHO is found or the current channel resumes. The DMM then recalculates the dwell time and updates the dwell timer. If no higher-order interruptions are found or the current channel does not resume during the dwell period, the UE sends a handover request message to the handover execution module (HEM) that resides in the network controller. Considering the network structure based on SDN platforms, the DMM can either resides in the UE or the network controller. The handover strategy is called mobile-controlled handover (MCHO) if the DMM resides in the mobile node while it is called mobile-assisted handover (MAHO) if the DMM locates in the network controller [37]. In the MAHO strategy, the information gathered needs to be reported to the DMM in the controller periodically via the uplink. This strategy is adopted in the handover scheme in [15]; however, it is not suitable for our handover scheme, since our adaptive dwell based algorithm utilises multiple attributes that would occupy

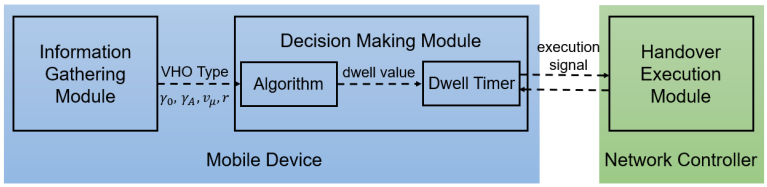

FIGURE 5. The proposed handover scheme with mobile-controlled handover (MCHO) strategy.

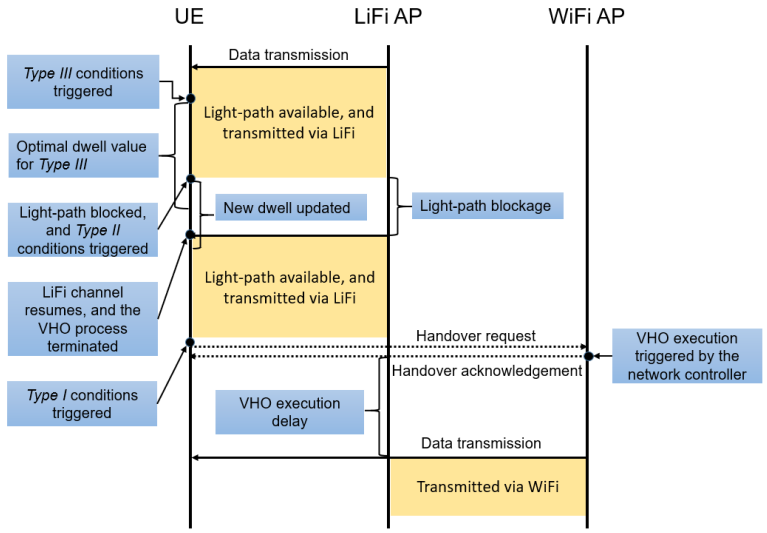

FIGURE 6. An example of a handover procedure from a LiFi AP to the WiFi AP.

too much WiFi channel resource to be sent to the controller. Therefore, the MCHO strategy is adopted and the DMM resides in mobile nodes in our study. The MCHO strategy can significantly reduce the handover reaction time and increase the efficiency of WiFi channel utilisation [37].

An example of a handover procedure from a LiFi AP to the WiFi AP is illustrated in Fig. 6. If the UE is at first connected to a LiFi AP, the dwell timer is initialized with a large enough value, *inf*. If *Type III* trigger conditions are satisfied, the IGM reports this to the DMM for dwell time calculation and timer setup. During the dwell time period, the IGM finds out that the optical channel is blocked, i.e. a *Type II* handover event occurs. It then sends this to the DMM again for the dwell time update. This handover process is terminated and the data transmission resumes when the LiFi channel is found to have recovered during the dwell period. After that, the *Type I* condition is satisfied and the dwell time is set as 0, which means to perform the handover immediately. The UE then sends a handover request message to the network controller via the WiFi uplink, and the handover is executed once the controller sends a handover acknowledgement message back to the UE. The UE is then transferred to the WiFi link after the execution delay, during which the buffer content is forwarded to the WiFi AP from the LiFi AP. The procedure of the handover from WiFi to LiFi is similar to that from LiFi to WiFi, except that there are only *Type III* VHOs in this situation, since WiFi is immune to user velocity, device rotation, or shadowing.

TABLE 1. LiFi Simulation Parameters.

Parameter	Value
Room size, $a \times b$	$18 \times 18m^2$
Height from desk to ceiling, h	$2.5m$
Number of APs, N_A	36
Semi angle of half power, $\phi_{1/2}$	60°
Transmitted optical power of LiFi AP α, $P_{t,\alpha}$	$9W$
Physical size of a PD, A_{pd}	$1cm^2$
Field of view, Ψ_{max}	90°
Optical gain, g_f	1
Refractive index of concentrator, n_i	1.5
Wall reflectivity, ρ_w	0.8
Optical to electric power conversion coefficient, ι	3
Detector responsivity, R_{pd}	$0.53A/W$
Noise PSD of LiFi channel, N_{LiFi}	$10^{-21}A^2/Hz$
Bandwidth of LiFi channel, B_{LiFi}	$40MHz$

IV. SIMULATION RESULTS

An asymmetric HLWNet system, as presented in Section II, has been built to compare the performance of the proposed adaptive handover algorithm and benchmarks. We choose three different handover schemes as benchmarks: the traditional IVHO and DVHO, and the FL based scheme [18]. We firstly implement the ORWP to gather indoor users' dynamic information. In the simulation, we assume that users keep stationary for 30% of the total simulation time, and move randomly in the rest of time; their velocity and movement direction for each step are uniformly distributed from $0 - 3$m/s and $0 - 2\pi$, respectively. The arrival

TABLE 2. WiFi Simulation Parameters.

Parameter	Value
Carrier frequency, f_c	$2.4GHz$
Transmitted power of WiFi AP, $P_{t,0}$	$20dBm$
Type of channel model	D
Breakpoint distance, d_{BP}	$10m$
Shadowing fading std. dev for LoS, σ_{SF}	$3dB$
Shadowing fading std. dev for NLoS, σ_{SF}	$5dB$
The arrival/departure angle of LoS component, ϕ_0	$45°$
Ricean K-factor for LoS, K	2
Ricean K-factor for NLoS, K	0
Noise PSD of WiFi channel, N_{WiFi}	$-174dBm/Hz$
Bandwidth of LiFi channel, B_{WiFi}	$20MHz$

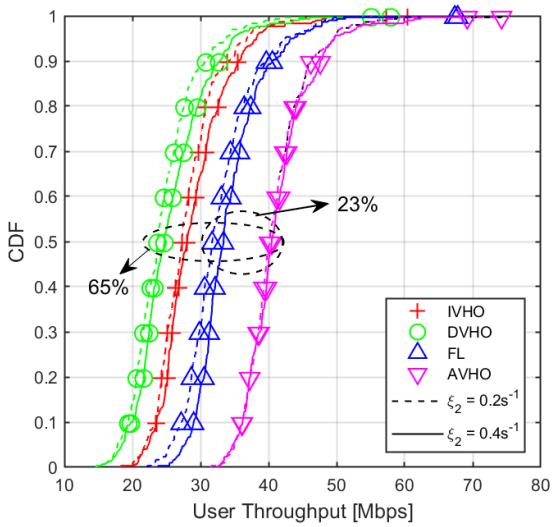

(a) $\xi_1 = 0.05\text{s}^{-1}$.

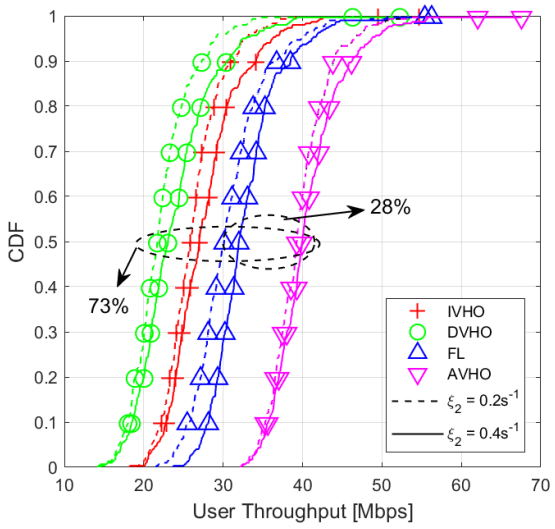

(b) $\xi_1 = 0.1\text{s}^{-1}$.

FIGURE 7. CDF plots of user throughput when the light-path interruption rate ξ_1 equals to (a) 0.05s^{-1} and (b) 0.1s^{-1}.

data rate follows a Poisson distribution with a mean value equivalent to 300Mbps [18] and the fixed packet length is 1K [38]. In addition, the delay of the VHO execution is approximated as a normal distribution with an expected value

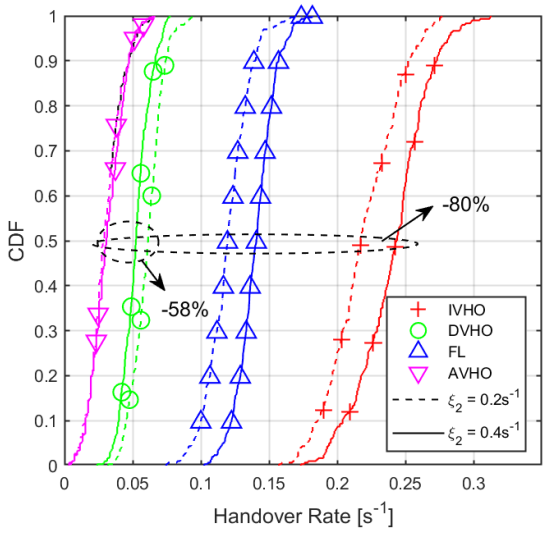

(a) $\xi_1 = 0.05\text{s}^{-1}$.

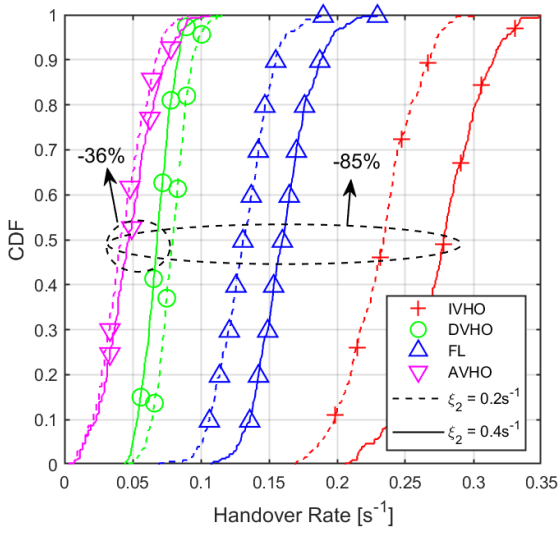

(b) $\xi_1 = 0.1\text{s}^{-1}$.

FIGURE 8. CDF plots of average handover rate when the light-path interruption rate ξ_1 equals to (a) 0.05s^{-1} and (b) 0.1s^{-1}.

of 400ms [12]. Additionally, $N_{U,0}$ and $N_{U,a}$ users, following Poisson distributions, are assumed to be connected to WiFi and the target LiFi AP at each time. 300 users are evaluated and each of them has a simulation time of 300s. Other simulation parameters are summarised in Table 1 and 2. All simulations were done in Matlab. In this section, the proposed handover algorithm, adaptive dwell based VHO (AVHO), is compared with IVHO, DVHO, and FL benchmarks in four aspects: user throughput, handover rate, robustness, and delay.

A. THROUGHPUT

Fig. 7 shows the cumulative distribution function (CDF) plots of user throughput under different channel conditions. The light-path blockage rate ξ_1 is set as 0.05s^{-1} and 0.1s^{-1} in

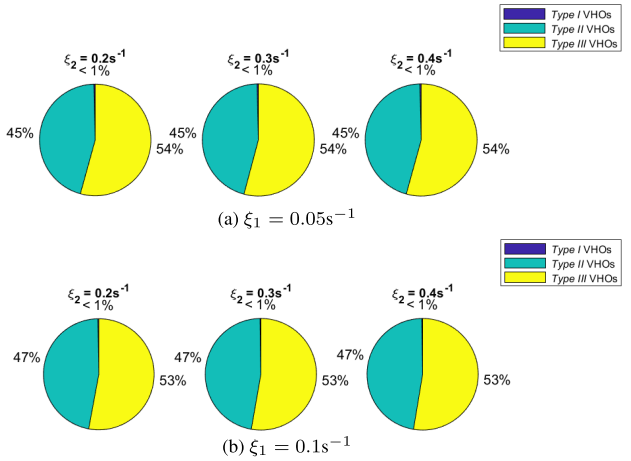

FIGURE 9. The proportion of different categories of VHOs when ξ_1 equals to (a) $0.05s^{-1}$, (b) $0.1s^{-1}$.

Fig. 7a and 7b respectively, whereas the light-path recovery rate varies from 0.2 to $0.4s^{-1}$. The performance of each algorithm under different channel conditions varies slightly; however, the performance is significantly different among different algorithms. The average user throughput provided by the AVHO method is always the highest and that of the FL method is the second highest. The UEs implemented with AVHO can achieve around $23-28\%$ higher throughput than those with FL scheme do. The throughput performance of IVHO and DVHO are quite similar and their throughput is the lowest. The user throughput of the proposed AVHO is roughly $65-73\%$ higher than that of DVHO.

B. HANDOVER RATE

In Fig. 8, the performance of handover rate is presented. The simulation is still carried out under different LiFi channel conditions set as in Section IV-A. It shows that the proposed algorithm achieves the lowest handover rate globally. Fig. 8a shows that the UEs implemented with AVHO have around 80% and 58% fewer VHOs than those with IVHO and DVHO methods. When the optical blockage rate increases from $0.05s^{-1}$ to $0.1s^{-1}$, AVHO method still reduces 85% and 36% more VHOs than IVHO and DVHO methods do. In addition, the performance of IVHO and FL fluctuates greatly as ξ_1 and ξ_2 vary, and that of DVHO also changes slightly; however, the change of AVHO is the smallest, which means that the proposed method has the strongest robustness as compared to the benchmarks. The robustness performance will be further discussed in the following subsection. The proportions of different categories of VHOs under different channel conditions are summarised in Fig. 9. It shows that the number of *Type I* VHOs is extremely low, which is because they are only triggered when the user velocity suddenly increases and exceeds the upper threshold. The proportions of *Type II* and *Type III* VHOs change slightly from 45% and 54% to 47% and 53% when ξ_1 increases from $0.05s^{-1}$ to $0.1s^{-1}$.

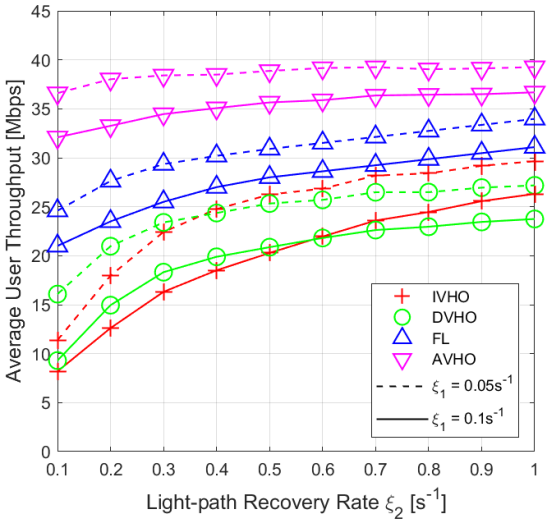

FIGURE 10. Robustness analysis of average user throughput against different channel qualities.

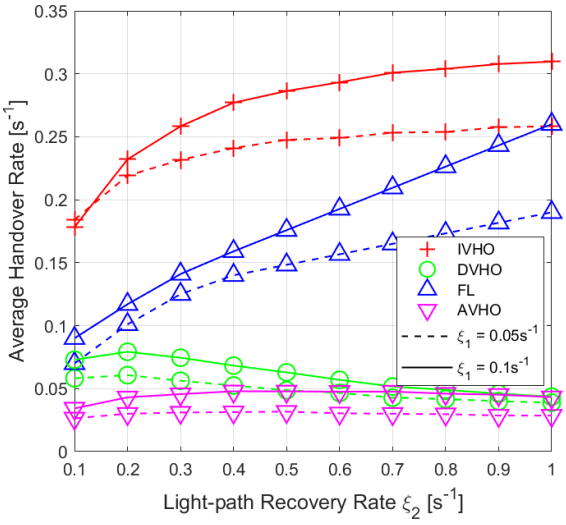

FIGURE 11. Robustness analysis of average handover rate against different channel qualities.

C. ROBUSTNESS

Fig. 10 and Fig. 11 present the average user throughput and handover rate performance of different handover methods under different channel qualities, which is determined by interruption and resumption rates of the LiFi channel. The interruption rate ξ_1 is chosen as $0.05s^{-1}$ and $0.1s^{-1}$, while the resumption rate ξ_2 ranges from $0.1s^{-1}$ to $1s^{-1}$. Fig. 10 shows that the average user throughput of the three methods all decline with the increase of the interruption rate ξ_1. Given a fixed interruption rate ξ_1, it is found that: i) the achievable data rate provided by AVHO is always higher than the benchmarks; and ii) The proposed method has the flattest curves, which indicates that our method has the best robustness. The numerical analysis of average user throughput is presented in Table 3 by checking the expected value and standard deviation. Compared to the benchmarks, our method has the highest mean value and lowest standard

TABLE 3. Numerical Analysis of Average User Throughput.

	$M \pm SD$[Mbps]		
VHO Algorithms	$\xi_1 = 0.05\text{s}^{-1}$	$\xi_1 = 0.1\text{s}^{-1}$	All
IVHO	23.5039 ± 5.8237	20.7810 ± 5.9344	22.1425 ± 5.8905
DVHO	23.2932 ± 3.4528	20.7936 ± 4.5708	22.0434 ± 4.1458
FL	30.6390 ± 2.8544	27.4270 ± 3.2356	29.0330 ± 3.3961
AVHO	38.6224 ± 0.8241	35.2394 ± 1.5398	36.9306 ± 2.1110

TABLE 4. Numerical Analysis of Average User Throughput.

	$M \pm SD[\text{s}^{-1}]$		
VHO Algorithms	$\xi_1 = 0.05\text{s}^{-1}$	$\xi_1 = 0.1\text{s}^{-1}$	All
IVHO	0.2396 ± 0.0230	0.2748 ± 0.0418	0.2572 ± 0.0375
DVHO	0.0487 ± 0.0079	0.0605 ± 0.0128	0.0546 ± 0.0120
FL	0.1451 ± 0.0376	0.1815 ± 0.0554	0.1633 ± 0.0497
AVHO	0.0298 ± 0.0016	0.0448 ± 0.0041	0.0373 ± 0.0083

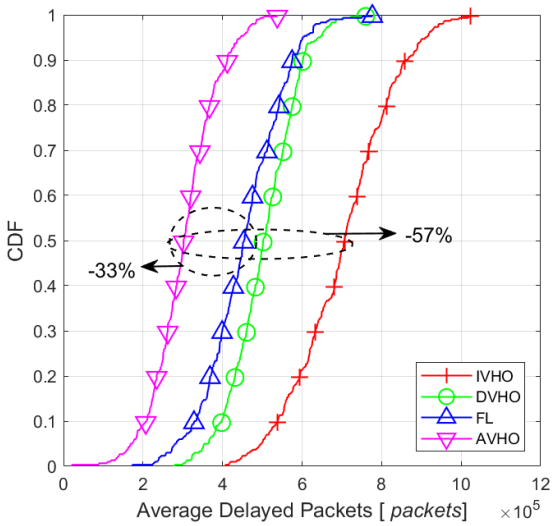

FIGURE 12. The CDF plot of average packet delay of four handover schemes.

deviation, which means that it is able to provide the highest data rate whilst maintaining the strongest robustness. Similarly, Fig. 11 shows that the average handover rate of AVHO and DVHO are similar and much lower than that of IVHO. The numerical results of the handover rate of these three methods are attached in Table 4, which shows that the proposed AVHO achieves the lowest handover rate and strongest robustness under different channel conditions.

D. DELAY

Another metric of interest to evaluate a handover scheme is delay, whose performance is very important for real time applications. The delay is determined by both the throughput and the handover rate. Generally speaking, higher user throughput and lower handover rate lead to less delay. The CDF plot of the average packet delay is presented in Fig. 12. Since the proposed AVHO achieves the highest user throughput and lowest handover rate, as we expected, it achieves the best delay performance. More specifically, the UEs implemented with the proposed AVHO handover scheme are able to reduce packet delay by 33% and 57% as compared with the FL and IVHO handover schemes. The delay performance of the DVHO is slightly worse than that of the FL method.

V. CONCLUSION

In this paper, a novel handover scheme has been proposed to boost the user throughput and reduce handover rate by applying optimal dwell time for individual VHO events. The VHOs in the HLWNet are divided into three categories and each of them applies a particular strategy to calculate dwell dime. Information about user velocity, SINR values, and arrival data rate is gathered by the IGM in the mobile node to decide if a VHO event has occurred and if so the type of the VHO. The related information is then sent to DMM to calculate the optimal dwell time and set up the dwell timer in it. The UE sends a handover request message to the HEM residing in the network controller once the set dwell time expires, and the VHO is executed after the HEM sends an acknowledge back to the UE. The simulation results show that the proposed algorithm can achieve global optimal performance on user throughput, handover rate, and packet delay as compared with IVHO, DVHO, and FL benchmarks. In addition, the proposed algorithm shows superior robustness performance as it can be adaptive to different working scenarios.

REFERENCES

[1] G. Forecast, "Cisco visual networking index: Global mobile data traffic forecast update, 2017–2022," *Update*, vol. 2017, p. 2022, Feb. 2019.
[2] H. Haas, L. Yin, Y. Wang, and C. Chen, "What is LiFi?" *J. Lightw. Technol.*, vol. 34, no. 6, pp. 1533–1544, Mar. 15, 2016.
[3] M. S. Islim, R. X. Ferreira, X. He, E. Xie, S. Videv, S. Viola, S. Watson, N. Bamiedakis, R. V. Penty, I. H. White, A. E. Kelly, E. Gu, H. Haas, and M. D. Dawson, "Towards 10 Gb/s orthogonal frequency division multiplexing-based visible light communication using a GaN violet micro-LED," *Photon. Res.*, vol. 5, no. 2, p. A35, 2017.

[4] H. Elgala, R. Mesleh, and H. Haas, "Indoor optical wireless communication: Potential and state-of-the-art," *IEEE Commun. Mag.*, vol. 49, no. 9, pp. 56–62, Sep. 2011.
[5] M. D. Soltani, H. Kazemi, M. Safari, and H. Haas, "Handover modeling for indoor Li-Fi cellular networks: The effects of receiver mobility and rotation," in *Proc. IEEE Wireless Commun. Netw. Conf. (WCNC)*, Mar. 2017, pp. 1–6.
[6] M. B. Rahaim, A. M. Vegni, and T. D. C. Little, "A hybrid radio frequency and broadcast visible light communication system," in *Proc. IEEE GLOBECOM Workshops (GC Wkshps)*, Dec. 2011, pp. 792–796.
[7] D. A. Basnayaka and H. Haas, "Hybrid RF and vlc systems: Improving user data rate performance of vlc systems," in *Proc. 81st Veh. Technol. Conf. (VTC Spring)*, 2015, pp. 1–5.
[8] M. Gudmundson, "Analysis of handover algorithms (microcellular radio)," in *Proc. 41st Veh. Technol. Conf.*, 1991, pp. 537–542.
[9] J. Márquez-Barja, C. T. Calafate, J.-C. Cano, and P. Manzoni, "An overview of vertical handover techniques: Algorithms, protocols and tools," *Comput. Commun.*, vol. 34, no. 8, pp. 985–997, Jun. 2011.
[10] A. M. Vegni and T. D. C. Little, "Handover in VLC systems with cooperating mobile devices," in *Proc. Int. Conf. Comput., Netw. Commun. (ICNC)*, Jan. 2012, pp. 126–130.
[11] F. Wang, Z. Wang, C. Qian, L. Dai, and Z. Yang, "Efficient vertical handover scheme for heterogeneous VLC-RF systems," *IEEE/OSA J. Opt. Commun. Netw.*, vol. 7, no. 12, pp. 1172–1180, Dec. 2015.
[12] J. Hou and D. C. O'brien, "Vertical handover-decision-making algorithm using fuzzy logic for the integrated radio-and-OW system," *IEEE Trans. Wireless Commun.*, vol. 5, no. 1, pp. 176–185, Jan. 2006.
[13] G. Ma, R. Parthiban, and N. Karmakar, "A comparison of IVHO and DVHO in heterogeneous VLC-RF networks," in *Proc. IEEE Region 10 Symp. (TENSYMP)*, Jeju Island, South Korea, Aug. 2021, pp. 1–7.
[14] R. Liu and C. Zhang, "Dynamic dwell timer for vertical handover in VLC-WLAN heterogeneous networks," in *Proc. 13th Int. Wireless Commun. Mobile Comput. Conf. (IWCMC)*, Jun. 2017, pp. 1256–1260.
[15] S. Shao, Z. Khan, G. Liu, A. Khreishah, M. Ayyash, H. Elgala, T. D. C. Little, and M. Rahaim, "Poster abstract: Optimizing handover parameters by Q-learning for heterogeneous RF-VLC networks," in *Proc. IEEE Conf. Comput. Commun. Workshops*, Apr. 2019, pp. 1069–1070.
[16] X. Wu and H. Haas, "Handover skipping for LiFi," *IEEE Access*, vol. 7, pp. 38369–38378, 2019.
[17] X. Wu, D. C. O'Brien, X. Deng, and J.-P.-M. G. Linnartz, "Smart handover for hybrid LiFi and WiFi networks," *IEEE Trans. Wireless Commun.*, vol. 19, no. 12, pp. 8211–8219, Dec. 2020.
[18] Y. Wang, X. Wu, and H. Haas, "Fuzzy logic based dynamic handover scheme for indoor li-fi and RF hybrid network," in *Proc. IEEE Int. Conf. Commun. (ICC)*, May 2016, pp. 1–6.
[19] X. Wu, M. D. Soltani, L. Zhou, M. Safari, and H. Haas, "Hybrid LiFi and WiFi networks: A survey," *IEEE Commun. Surveys Tuts.*, vol. 23, no. 2, pp. 1398–1420, 2nd Quart., 2021.
[20] D. Kreutz, F. Ramos, P. E. Veríssimo, C. E. Rothenberg, S. Azodolmolky, and S. Uhlig, "Software-defined networking: A comprehensive survey," *Proc. IEEE*, vol. 103, no. 1, pp. 14–76, Jan. 2015.
[21] H. Alshaer and H. Haas, "SDN-enabled Li-Fi/Wi-Fi wireless medium access technologies integration framework," in *Proc. IEEE Conf. Standards for Commun. Netw. (CSCN)*, Oct. 2016, pp. 1–6.
[22] Z. Zeng, M. Dehghani Soltani, Y. Wang, X. Wu, and H. Haas, "Realistic indoor hybrid WiFi and OFDMA-based LiFi networks," *IEEE Trans. Commun.*, vol. 68, no. 5, pp. 2978–2991, May 2020.
[23] J. M. Kahn and J. R. Barry, "Wireless infrared communications," *Proc. IEEE*, vol. 85, no. 2, pp. 265–298, Feb. 1997.
[24] M. D. Soltani, A. A. Purwita, Z. Zeng, H. Haas, and M. Safari, "Modeling the random orientation of mobile devices: Measurement, analysis and LiFi use case," *IEEE Trans. Commun.*, vol. 67, no. 3, pp. 2157–2172, Mar. 2019.
[25] C. Chen, D. A. Basnayaka, and H. Haas, "Downlink performance of optical attocell networks," *J. Lightw. Technol.*, vol. 34, no. 1, pp. 137–156, Jan. 1, 2016.
[26] Z. Ghassemlooy, W. Popoola, and S. Rajbhandari, *Optics Wireless Communications: System Channel Modeling With MATLAB*. Boca Raton, FL, USA: CRC Press, 2019.
[27] X. Li, R. Zhang, and L. Hanzo, "Cooperative load balancing in hybrid visible light communications and WiFi," *IEEE Trans. Commun.*, vol. 63, no. 4, pp. 1319–1329, Apr. 2015.
[28] E. Perahia and R. Stacey, *Next Generation Wireless LANs: 802.11 n and 802.11 Ac*. Cambridge, U.K.: Cambridge Univ. Press, 2013.
[29] J.-B. Wang, Q.-S. Hu, J. Wang, M. Chen, and J.-Y. Wang, "Tight bounds on channel capacity for dimmable visible light communications," *J. Lightw. Technol.*, vol. 31, no. 23, pp. 3771–3779, Dec. 1, 2013.
[30] X. Wu and D. C. O'Brien, "Parallel transmission LiFi," *IEEE Trans. Wireless Commun.*, vol. 19, no. 10, pp. 6268–6276, Oct. 2020.
[31] A. A. Purwita, M. D. Soltani, M. Safari, and H. Haas, "Terminal orientation in OFDM-based LiFi systems," *IEEE Trans. Wireless Commun.*, vol. 18, no. 8, pp. 4003–4016, Aug. 2019.
[32] M. D. Soltani, M. A. Arfaoui, I. Tavakkolnia, A. Ghrayeb, M. Safari, C. M. Assi, M. O. Hasna, and H. Haas, "Bidirectional optical spatial modulation for mobile users: Toward a practical design for LiFi systems," *IEEE J. Sel. Areas Commun.*, vol. 37, no. 9, pp. 2069–2086, Sep. 2019.
[33] D. Gross, *Fundamentals Queueing Theory*. Hoboken, NJ, USA: Wiley, 2008.
[34] S. Liang, H. Tian, B. Fan, and R. Bai, "A novel vertical handover algorithm in a hybrid visible light communication and LTE system," in *Proc. IEEE 82nd Veh. Technol. Conf. (VTC-Fall)*, Sep. 2015, pp. 1–5.
[35] H. J. Wang, R. H. Katz, and J. Giese, "Policy-enabled handoffs across heterogeneous wireless networks," in *Proc. 2nd Workshop Mobile Comput. Syst. Appl.*, 1999, pp. 51–60.
[36] M. Kassar, B. Kervella, and G. Pujolle, "An overview of vertical handover decision strategies in heterogeneous wireless networks," *Comput. Commun.*, vol. 31, no. 10, pp. 2607–2620, Jun. 2008.
[37] M. Zekri, B. Jouaber, and D. Zeghlache, "A review on mobility management and vertical handover solutions over heterogeneous wireless networks," *Comput. Commun.*, vol. 35, no. 17, pp. 2055–2068, Oct. 2012.
[38] J. D. Spragins, J. L. Hammond, and K. Pawlikowski, *Telecommunications: Protocols and Design*. Reading, MA, USA: Addison-Wesley, 1991.

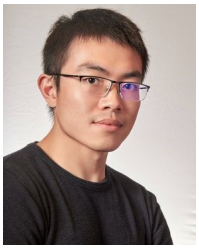

GUANGHUI MA (Graduate Student Member, IEEE) received the bachelor's degree in electrical engineering from Xi'an Jiaotong University, China, in 2016, and the master's degree (Hons.) in engineering from the University of Melbourne, in 2018. He is currently pursuing the Ph.D. degree with Monash University, Australia.

His research interests include visible light communication, heterogeneous optical, and RF networks.

RAJENDRAN PARTHIBAN (Senior Member, IEEE) received the Bachelor of Engineering (Hons.) and Ph.D. degrees in optical networks from the University of Melbourne, Australia, in 1997 and 2004, respectively.

He joined as a Lecturer at the School of Engineering, Monash University Malaysia, in 2006, where he is currently a Professor and has been serving as the Deputy Head of the School (academic), since August 2010. He has over 80 journal and conference publications. He obtained external grants worth over RM 2 million. Under his supervision, 12 Ph.D. and one master's degree students have completed their studies. His research interests include optical networks, visible light communications, vehicular communication, and engineering education.

Dr. Parthiban is a Senior Member of the Optical Society (OSA).

NEMAI KARMAKAR (Senior Member, IEEE) received the master's degree in electrical engineering from the University of Saskatchewan, Canada, in 1991, and the Ph.D. degree from The University of Queensland, Australia, in 1999.

He has over 20 years of teaching, design, and development experience in antennas, microwave active and passive circuits, and RFIDs in Canada, Australia, and Singapore. He is currently an Associate Professor with the Department of Electrical and Computer Systems Engineering, Monash University, Australia. He has authored or coauthored over 400 refereed journal and conference papers, 24 book chapters, and eight books. His research interests include RFID, smart antennas for mobile and satellite communications, the Internet of Things (IoT), and visible light communication.